Mössbauer and Raman spectroscopic study of oxidation and reduction of iron oxide nanoparticles promoted by various carboxylic acid layers

S.W. da Silva[1], L.R. Guilherme[1], A.C. de Oliveira[1], V.K. Garg[1], P.A.M. Rodrigues[1], J.A.H. Coaquira[1], Q. da Silva Ferreira[1], G.H.F. de Melo[1], A. Lengyel[2], R. Szalay[2], Z. Homonnay[2], Z. Klencsár[3], Gy. Tolnai[3], E. Kuzmann[2,*]

[1]Department of Physics, University of Brasília, Brasília, DF, Brazil
[2]Institute of Chemistry, Eötvös Loránd University, Budapest, Hungary
[3]Research Centre for Natural Sciences, Hungarian Academy of Sciences, Budapest, Hungary

Abstract. The effect of coating with nine different carboxylic acids (glycolic, propionic, lactic, malic, tartaric, citric, mandelic, caproic and caprylic) on nanostructured magnetite ($D \approx 10$ nm) was studied by Raman and photoacoustic, magnetic and ^{57}Fe Mössbauer measurements. Mössbauer spectra of frozen suspensions showed dominantly magnetically split envelopes at lower temperatures, which were evaluated by hyperfine field distribution method. Mössbauer and Raman spectroscopy indicated similar variation of relative occurrence of magnetite and maghemite phases. These results are discussed on the basis of the hypothesis that different carboxylic acids can promote either the oxidation or reduction of iron oxide nanoparticles.

Introduction

In the last few decades nanoparticles have attracted serious scientific and industrial interest since they can have very favorable and unique properties [1]. Iron oxide nanoparticles are subject of diverse research, including magnetic resonance imaging [2], high gradient magnetic separation (HGMS) [3], drug delivery [4,5] and various possible applications in material sciences and electronics [6]. In these applications, nanoparticles can help boost the resolution in magnetic tomographs, and they may find use in the mandatory cleaning of drinking water from colloidal particles and bacteria [7]. Further applications include biomedical ones such as novel therapies based on magnetically guided drug delivery [8], as well as some even more exotic applications in connection with ferrofluids [9] and their functionalized counterparts [10]. Iron-based nanoparticles are generally considered as non-toxic [11], however, some studies suggest they are potentially hazardous to health [12,13].

The formation [14] of iron oxide nanoparticles can proceed via chemical methods like co-precipitation [15] and thermal decomposition [16], as well as by physical methods such as grinding in ball-mills [17], laser ablation [18] or more exotic processes, like electric explosion of wire (EEW) [19]. In addition, biosynthetic methods are also known [20,21] for iron oxide nanoparticles. In this research we used a modified Khalafalla co-precipitation method [22] which can provide magnetite nanoparticles with small size and narrow particle size distribution.

* Corresponding author, kuzmann@caesar.elte.hu

In early studies of carboxylic acid coated nanomagnetites it has already been established that carboxylic (e.g., oleic) acids with long carbon chains give stable colloids [23]. In recent studies even certain carboxylic acids with short carbon chains (e.g., tartaric, citric acid), also provided stable colloidal solutions of coated nanomagnetites [24, 25]. Studying the bonding between the carboxylic group and the nanomagnetite, Raman spectroscopy results showed the disappearance of C=O and the formation of a new C–O bond [26]. Recent studies also suggest that -OH groups can also contribute to the bonding process [27]. Properties of the nanocomposites, like water solubility [28], size of particles aggregates [29], colloidal stability [30] as well as magnetism [31], can also depend on the nature of the carboxylic acid constituting the coating layer.

The most accepted model for magnetite nanoparticles is the core-shell model, where the core of the nanoparticle consists of magnetite, while the shell consists of maghemite [32]. Under certain conditions the magnetite core can transform into maghemite. The oxidation mechanism that is hypothesized to be responsible for the transformation, assumes diffusion of iron atoms within the crystal [33]. This transformation can be monitored by various methods, such as Raman [34], Mössbauer [35], and X-ray spectroscopy [36] as well as magnetic methods [37]. For organic base coatings changes in magnetite/maghemite ratio were found to correlate to the carbon chain length [38]. However, the effect of the bonding of different carboxylic acids with the system of iron oxide and carboxylic acid on the maghemite/magnetite ratio has not been studied yet. Continuing our previous studies on different iron oxide ferrofluids and nanocomposites [23,39,40], and, furthermore, the preparation and characterization of magnetite nanoparticles coated with various carboxylic acids of short carbon chains, our aim was to determine the maghemite/magnetite ratio of the nanoparticles, and to explore possible correlations between the maghemite/magnetite ratios and the nature of the carboxylic acid bonded to the nanoparticles.

Materials and experimental methods

Sample preparation

Based on the early work of Khalafalla [22] for the synthesis of nanomagnetite, 24 g of $FeCl_3 \cdot 6H_2O$ and 12 g of $FeCl_2 \cdot 4H_2O$ were dissolved in 100 ml of water with vigorous stirring at 20°C under ambient atmosphere. (15% of excess $FeCl_2$ over the stoichiometric amount was applied to reckon upon the possible oxidation since the preparation occurred in air atmosphere). Then 10 ml of NH_4OH (28 m/ m%) was quickly added to the mixture and stirring was continued for 30 min. The obtained particles were washed with deionized water under stirring for 10 cycles. In contrast to previous studies, we separated the synthetic and the functionalization steps from each other. For each functionalization with carboxylic acid a mass fixed (1 g) of freshly synthesized nanomagnetites was put in a reactor, then were coated by adding carboxylic acid dissolved in NH_4OH (28 m/m% NH_3 in H_2O, 1 mol NH_3 for 1 mol -COOH group). Then the reaction mixture was heated up to 60ºC during vigorous stirring for 60 min. The separation of the magnetic coated particles was performed with a neodymium magnet. To remove excess carboxylic acids, the samples were washed with deionized water for three times. The coated nanomagnetites were stored at pH 7 as aqueous suspension.

Experimental methods

The transmission electron microscopy measurements of samples were carried out with a JEOL 100CXII electron microscope at room temperature. A drop of the colloid samples containing about 3×10^{-5} % volume fraction was deposited on the sample holder (a 300 mesh copper grid covered with formvar) and dried on air at room temperature before the TEM pictures were taken.

The magnetic characterization was performed using a vibrating sample magnetometer (VSM) module of a physical properties measurements system (PPMS-6000 from Quantum Design). Zero field cooled (ZFC) and field cooled (FC) susceptibility measurements were performed by cooling the sample from 300 to 5 K in zero field, and the magnetic moment was determined as the sample was warmed up in a magnetic field of 50 Oe.

The ^{57}Fe Mössbauer measurements of nanoparticles were carried out with a conventional constant acceleration (WISSEL) Mössbauer spectrometer using integrated multichannel analyzer and scintillation detection in transmission geometry. The colloid samples were measured in a frozen state at 78 and 5 K temperatures by the means of a JANIS liquid helium cryostat at 78 K and at 5 K by applying liquid He as coolant. In addition, Mössbauer spectra of the dried samples were also recorded at 295 K. ^{57}Co source of 0.8 GBq activity in Rh matrix supplied the gamma rays. The isomer shift values are given relatively to α-iron at room temperature. The analysis of the Mössbauer spectra was carried out with the MOSSWINN 4.0 code [41].

The Raman spectra were recorded using a commercial Jobin–Yvon triple spectrometer (T64000) equipped with a CCD detector. The 514 nm line of a CW Argon ion laser was used to excite the samples whereas the optical excitation intensity was kept around 0.2 mW. All Raman measurements were performed at room temperature.

The photoacoustic (PA) spectroscopic data were recorded at room temperature with the samples enclosed in a sealed, home-made PA cell, at ambient pressure and coupled to a sensitive microphone [42]. The PA spectra were recorded using the light from a 150 W Xe lamp dispersed by a SPEX 1681B monochromator and scanning in the visible and near infrared range (350-1000 nm). The light was chopped at a frequency of a few hertz to improve the signal to noise ratio.

Results and discussion

Particle size and morphology by transmission electron microscopy

Transmission electron micrographs (Fig. 1a) show the morphology of two nanomagnetite samples. The particle size of nanoparticles is approximately 10 nm with a size distribution between 5 and 15 nm (Fig. 1b). These values are consistent with the results of the Mössbauer measurements. The TEM results provide evidence for the successful preparation of nanoparticles with a size similar to that reported in [24, 25].

Particle size estimation by Mössbauer spectroscopy

Mössbauer spectroscopy also can be used to estimate the particle size of magnetic nanoparticles. Magnetic relaxation, and particularly superparamagnetism (SPM), is a key feature of magnetic nanoparticles arising in connection with their size being smaller than a characteristic limit

that is typically below a few tens of nanometers. In biomedical in vivo applications it is important that below this critical particle size, magnetic interaction driven agglomeration of nanoparticles is absent [43].

Typical Mössbauer spectra of dried caprylic acid coated nanomagnetite samples recorded at room temperature and at 5 K are illustrated in Fig. 2. The Mössbauer spectra of these nanocomposites exhibit a sextet line envelope due to the magnetic splitting of nuclear sublevels of ^{57}Fe caused by the hyperfine magnetic interaction associated with the ferrimagnetic state of magnetite at room temperature [44].

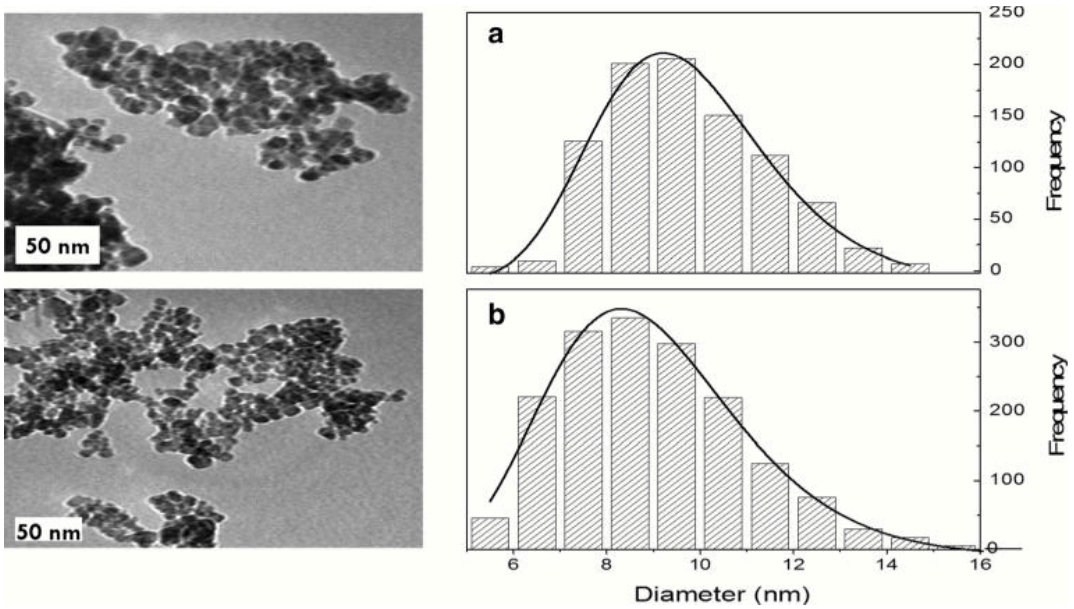

Fig. 1. Transmission electron micrographs (left) and corresponding size distributions (right) of uncoated (**a**) and propionic acid coated (**b**) iron-oxide nanoparticles.

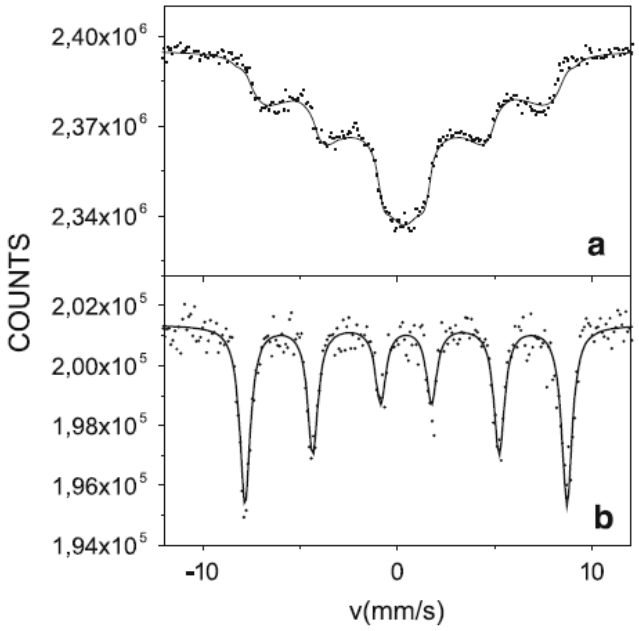

Fig. 2. ^{57}Fe Mössbauer spectra of caproic acid coated nanomagnetites recorded at room temperature (**a**) and at 5 K (**b**).

However, in contrast with the case of bulk magnetite that is characterized with narrow-peak sextets with well-defined Mössbauer parameters [45], the spectra of the present samples display absorption peaks with considerable line broadening.

The observed line broadening and spectrum envelope can be accounted for by assuming superparamagnetic relaxation of nanoparticle magnetic moments with a relaxation frequency of a few times of 10^7 Hz. The shape of the spectra, and particularly the absence of a superparamagnetic singlet or doublet component, reflect that the anisotropy energy barrier, $E_a \approx KV$ (where K is the volumetric anisotropy energy density and V is the particle volume), and thus the particle size is quite uniform in our samples, in good agreement with Fig. 1. Low-temperature Mössbauer measurements carried out at 5 K (Fig. 2b) provide further confirmation of the decisive role of magnetic relaxation in the line broadening observed in the room-temperature spectra (Fig. 2a). Namely, the decrease of temperature clearly leads to a narrowing of the absorption peaks as expected for a system of nanoparticles susceptible to thermally induced relaxation of their magnetic moments. The relaxation model fit of the Mössbauer spectra at different temperature allow to estimate the particle size [46] around 10 nm in agreement with the results of electron microscopy measurements.

Magnetite/maghemite ratio derived by Mössbauer spectroscopy

78 K Mössbauer spectra of nano-iron-oxides coated with different carboxylic acids are shown in Fig. 3. The envelop of the spectra shows a six-line pattern. These Mössbauer spectra can be decomposed into subspectra based on a model dependent evaluation method that requires the a priori knowledge of constraints among parameters (position, width, amplitude, line shape) of the spectral lines. In the case of magnetite nanoparticles, however, various factors (e.g., relaxation effect of superparamagnetic particles, change in Wervey temperature, non-stochiometry) may cause uncertainty in the application of the model dependent decomposition and in the exact determination of Mössbauer parameters, especially for the quantitative analysis of different species.

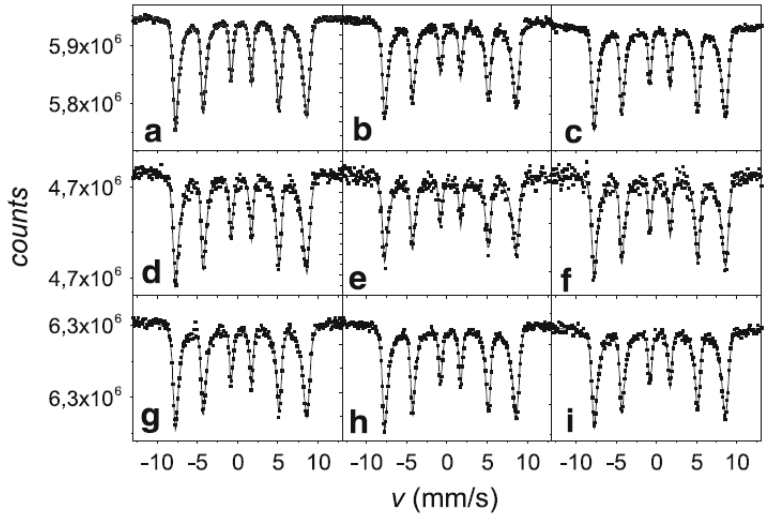

Fig. 3. Our fitting method applied to Mossbauer spectra of all of our samples, **a** caproic; **b** caprylic; **c** pristine; **d** malic; **e** lactic; **f** mandelic; **g** tartaric; **h** glycolic; **i** propionic acid coated nanomagnetites.

In order to determine the changes in maghemite/magnetite ratio we used the model independent technique, such as the hyperfine field distribution method (Hesse-Rübartsch method [47]) for the Mössbauer spectrum evaluation. The solid lines in Fig. 3 represent the fitted spectra. By this method, we can find the magnetic field components associated with the most probable iron microenvironments (characteristic of magnetite and maghemite) without using any model or restriction for the spectrum analysis. Figure 4 shows the hyperfine field distributions of the nanomagnetites coated with carboxylic acids. The highest field peak (red component in Fig. 4) is associated with maghemite, while the lower field peaks reflect magnetite (blue component in Fig. 4). The relative area of the peaks in the hyperfine field distributions can be used to derive quantitative analytical information about the components in the samples. The difference in maghemite/magnetite ratios between the carboxylic acid coated and uncoated (pristine) samples, obtained from the above-mentioned evaluation of the Mössbauer spectra are shown in Fig. 8 in comparison with the result of Raman method. It can be seen that nanomagnetite coated with carboxylic acids like tartaric-, propionic-, glycolic-, malic- and caproic acids exhibit smaller maghemite/magnetite ratio than that of pristine while coating with carboxylic acids like mandelic-, caprylic- and lactic acids increase maghemite/magnetite ratio compared to that of pristine nanomagnetite.

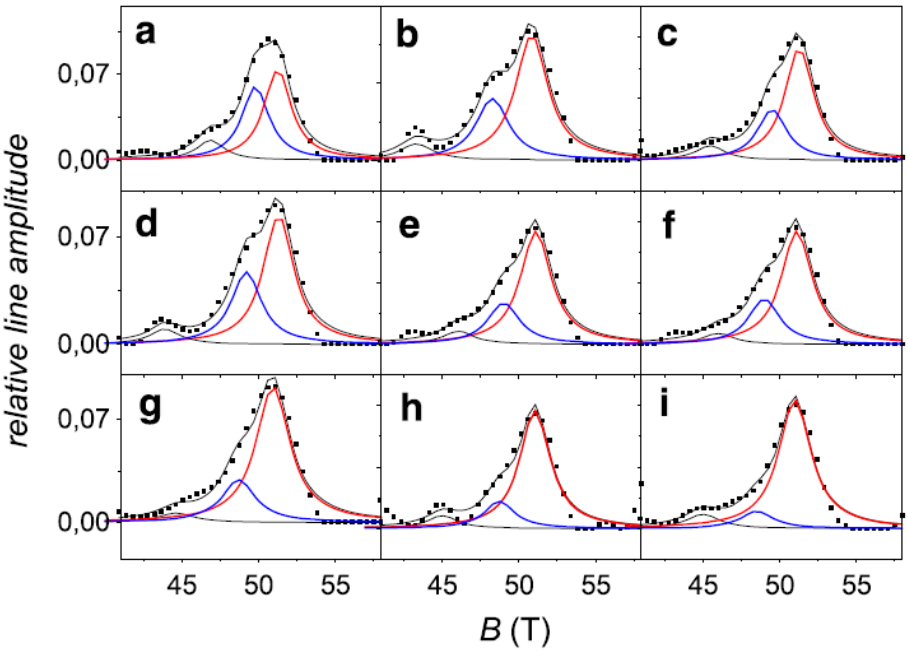

Fig. 4. Hyperfine field distributions for all of our Mossbauer spectra, **a** propionic; **b** malic; **c** glycolic; **d** tartaric; **e** pristine; **f** caproic; **g** caprylic; **h** lactic; **i** mandelic acid coated nanomagnetites.

Magnetite/maghemite ratio derived by Raman spectroscopy Raman spectroscopy can directly measure the ratio of tetrahedral and octahedral states in the crystal therefore it gives the maghemite/magnetite ratio [48]. All of the investigated short carbon chained carboxylic acids can be bound to the surface of iron oxide nanoparticles. This is directly proven by IR spectroscopy (not shown here), which indicates the disappearance of the absorption peak of the C=O stretch at 1700 cm^{-1}. The absence of these bands is an evidence of the adsorption of the carboxylic acids around the nanoparticle. Figure 5 presents the room temperature Raman spectra of carboxylic acid coated nanomagnetites together with the pristine sample recorded in the range of 150-800 cm^{-1}.

The Raman features indicated in Fig. 5 are the vibrational modes typical to the nanoparticles' crystalline structure. The fitting procedures, using Lorentzian-like lines, showed the presence of five structures around 175, 350, 515, 685 and 725 cm^{-1} for all samples. The peaks can be identified considering the Raman active symmetry modes expected for a cubic spinel (Fd3m) space group [49]. For the magnetite the correspondent modes are A_{1g} (685 cm^{-1}), T_{2g} (175 and 515 cm^{-1}) and E_g (350 cm^{-1}). Despite being structurally identical, the Raman spectra of magnetite and maghemite show marked differences. In general, of the maghemite presents Raman spectrum with broad and shifted bands to higher energies as compared with magnetite spectrum. It is found that the A_{1g} mode appears around 685 cm^{-1} for magnetite and around 720 cm^{-1} for maghemite [48,49].

According to literature the vibrational mode in higher energy, with A_{1g} symmetry, is associated to the stretching vibrational mode of the Fe^{3+} ions in A-sites which are surrounded by four nearest O^{2-} ions, each one bounded to the nearest B-sites occupied by twelve Fe^{3+}/Fe^{2+} ions $Fe^{A}—O_4—Fe^{B}_{12}$). Oxidation of Fe^{2+} to Fe^{3+} in magnetite leads to a cation-deficiency in B-sites, resulting in the formation of the maghemite. It is precisely the presence of the vacancy in B-sites, resulting at bond ($Fe^{A}—O_4—(Fe_8\square_4)^{B}$) in which □ represents vacancies, the responsible by Raman shift of 685 cm^{-1} (magnetite) to 720 cm^{-1} (maghemite). Once the integrated intensity of this Raman mode is proportional to the number of the corresponding oscillators is possible estimate the maghemite/magnetite ratio by taking the ratio between integrated areas associated to modes around 725 (black) and 685 cm^{-1} (light gray) [48]. This is also indirectly supported by Raman results indicating that we can find an order of carboxylic acids as an effect of bonding of nanomagnetite with different carboxylic acids. These changes also serve as an evidence of the existence of the carboxylic acid coating layer on the surface of nanomagnetites. The results for maghemite/magnetite ratio obtained from the Raman spectra (Fig. 5) corresponds well to those derived from Mössbauer results, thereby confirming the latter.

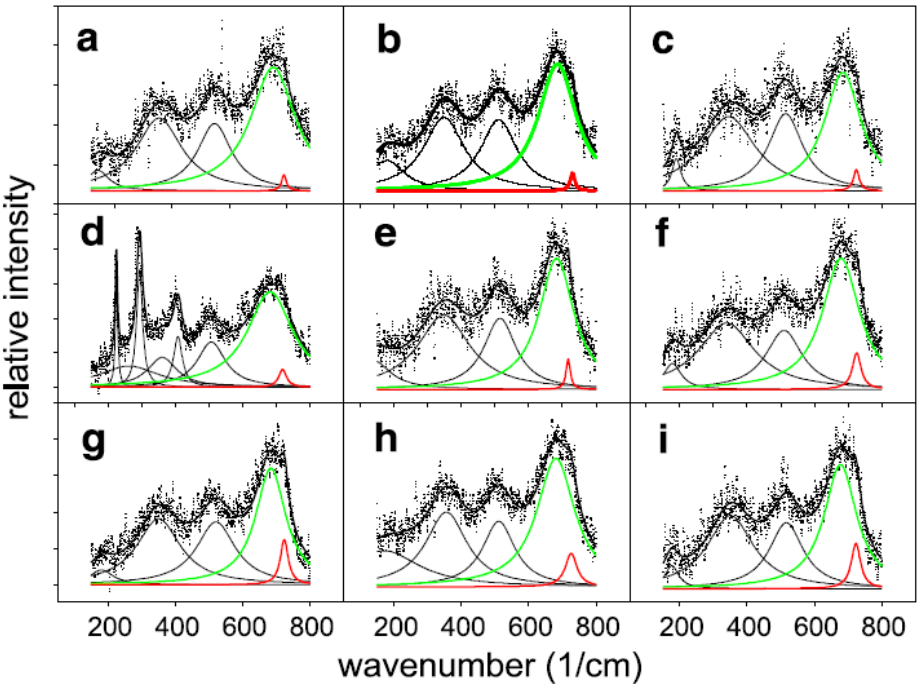

Fig. 5. Region of Raman spectra characteristic for the changes in magnetite/maghemite ratios for our samples, **a** propionic; **b** malic; **c** glycolic; **d** tartaric; **e** caproic; **f** pristine; **g** caprylic; **h** lactic; **i** mandelic acid coated nanomagnetites.

Supporting results by magnetization measurements and photoacoustic spectroscopy

Magnetization measurements

Figure 6 shows hysteresis and FC as well as ZFC curves for selected carboxylic acid coated nanomagnetites. The superparamagnetic nature of these samples is confirmed by the observation of thermal blocking in temperature-dependent FC, ZFC magnetization curves. We found that the saturation magnetizations of the caprylic acid coated nanomagnetite and the pristine sample are 50.0 and 70.0 emu/g. These values are lower than the reported one for bulk Fe_3O_4, 90 emu/g [50], but consistent with measurements on other nanoparticle samples [28]. The reduction in MS can be attributed to the presence of a likely magnetically disordered maghemite shell. The value of the reduction of MS, correlates to the increased relative maghemite quantity, showing that the caprylic acid coated nanomagnetite have higher maghemite/magnetite ratios corresponding and further proving the validity of Mössbauer, Raman, and photoacoustic results.

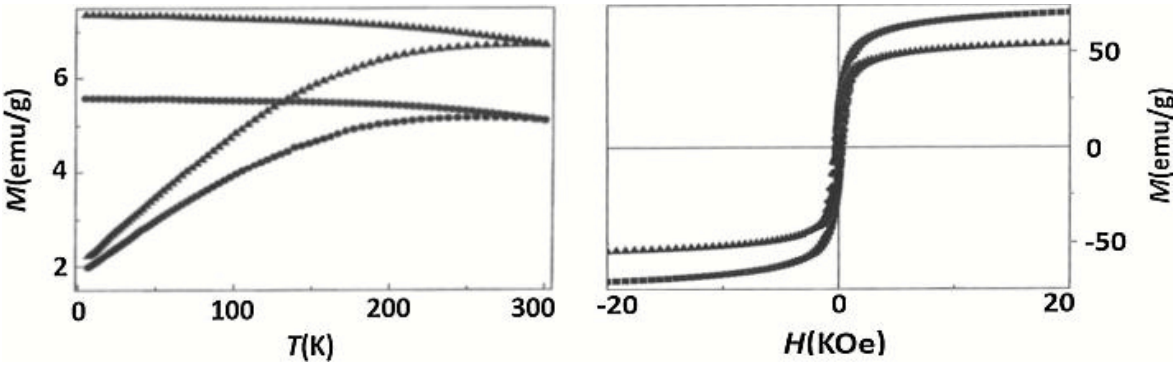

Fig. 6. FC and ZFC curve of caprylic acid coated nanomagnetites (dots) and pristine sample (triangles) at 50 Oe (left), magnetization versus magnetic field curve of caprylic acid coated nanomagnetite (triangles) and pristine sample recorded at 300 K (right).

Photoacoustic spectroscopy measurements

Magnetite is known to be a strong optical absorber in the visible region with a structureless absorption spectrum [33, 51]. In the near infrared range it has a very broad absorption band centered at ~ 1400 nm (0.9 eV) that goes down to 800 nm. This band is associated with intervalence charge transfer (IVCT) transitions [33]. Maghemite is a semiconductor with a band gap of ~ 2 eV but as there are Fe d-d transitions below the fundamental gap, the band edge absorption is not observed. However, the optical absorption of maghemite decreases strongly for $\lambda > 700$ nm [51]. Actually, Tang et al. [33] were able to use the absorption band of magnetite at ~ 1400 nm to study the oxidation of Fe_3O_4 nanoparticles to maghemite. Figure 7 shows the photoacoustic (PA) spectra of two of the Fe_3O_4 samples coated with the carboxylic acids. As common in PA spectroscopy, the recorded signal herein reported was divided by the PA signal of a black absorber to remove spectral variations due to the light source, optics etc. [52]. The PA signal shown in Fig. 7 is proportional to the absorption coefficient [52]. The PA signal recorded from all samples have been normalized at 350 nm (3.54 eV), well above the fundamental band gap of the bulk maghemite at ~ 2 eV [33]. It can be seen in Fig. 7 that the PA spectrum of the glycolic acid-coated sample is almost structureless in the range 350-1000 nm, however, there is only a small

decrease in the absorption coefficient around 650 nm. This minimum at ~ 650 nm is deeper for the caprylic acid-coated sample. The absorption of the two samples increase in the range 650-1000 nm suggesting the presence of the near infrared band of magnetite (IVCT transitions). The changes in maghemite/magnetite ratio can also be estimated from the photoacoustic spectra. The decreasing spectral intensity around 650 nm (Fig. 7) represents the relative increase of the maghemite phase. The observed changes in maghemite/magnetite ratio with the carboxylic acids correspond to the Mössbauer and Raman results and further confirm our findings.

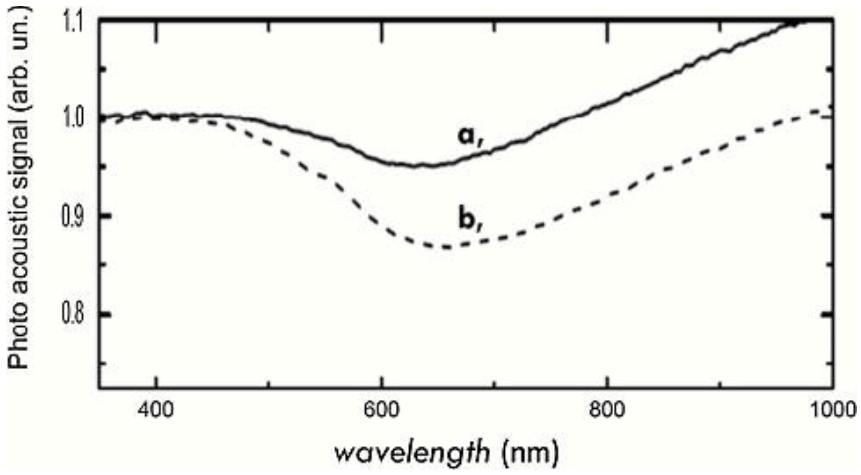

Fig. 7. Derivation of the maghemite/magnetite ratio increase from photoacoustic spectrum; **a** glycolic acid; **b** caprylic acid coated nanomagnetites.

Discussion

The characteristic features obtained by TEM, Raman, Mössbauer, and photoacoustic spectroscopy, and magnetic measurements, on the one hand, reveal the successful fabrication of carboxylic acid coated as well as uncoated nanomagnetites with 10 nm particle size, and, on the other hand, they are consistent with those reported earlier for available nanomagnetites [24,25]. In this study, the range [24,25] of various carboxylic acids with short carbon chain being able to stabilize nanomagnetite was considerably widened.

It was found with Mössbauer, Raman and photoacoustic spectroscopy that these nanoparticles consist both magnetite and maghemite phases that further supports the core/shell model [32] for these nanomagnetites. In our cases the thickness of maghemite shell can be estimated to be 1-2 nm which is a similar value found by Frison et al. [53] for certain acids.

Without any protective layer nanomagnetite will be oxidized to nanomaghemite (and thus changing its physical properties and applicability) in air. A certain degree of this oxidation process occurs during the preparation of the pristine nanomagnetite sample. The further oxidation of nanomagnetite was prevented by a protective NH_4^+ layer (originated from the ammonium salt solution), resulting in the obtained maghemite/magnetite ratio in pristine sample.

The addition of the carboxylic acid solution to the pristine sample removes the NH_4^+ layer, and then the formation of bonds between carboxylic acids and iron oxide nanoparticles begins. In this reaction either oxidation or reduction of iron oxide nanoparticles can occur. Our results for maghemite/magnetite ratios can be interpreted in terms of these processes. In Fig. 8 the increase of the maghemite/magnetite ratios of the carboxylic acid coated and uncoated (pristine) samples,

obtained from both the Mössbauer and the Raman results, determines an order of the carboxylic acids. The increase of maghemite/magnetite ratio indicates oxidation, while its decrease reflects reduction relatively to maghemite/magnetite ratio of pristine. Consequently, the correlation between of the maghemite/magnetite ratio and the order of carboxylic acids (Fig. 8) can lead to the conclusion that carboxylic acids, such as mandelic, caprylic and lactic acids, can promote oxidation of nanomagnetites, contrasted to carboxylic acids, such as tartaric, propionic, glycolic, malic and caproic acids, which promote the reduction of iron oxide nanoparticles. The same tendency of the relationship between maghemite/magnetite ratios and carboxylic acids were found simultaneously by Mössbauer, photoacoustic and Raman spectroscopy and magnetic measurements. The effect of carboxylic acids as oxidation or reduction process of the nanomagnetite can also be illustrated as an increase or decrease of the thickness of the maghemite shell, respectively, as demonstrated in Fig. 9.

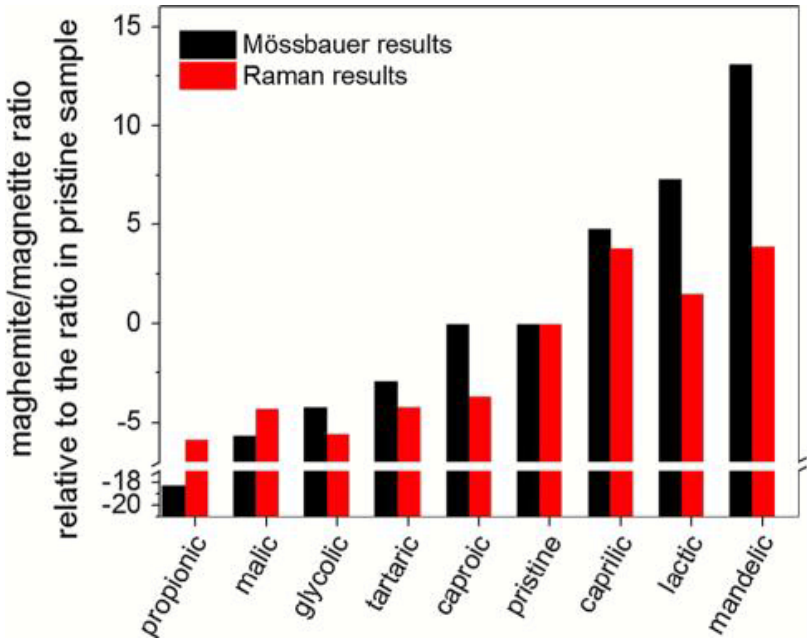

Fig. 8. Correlation between maghemite/magnetite ratio in coated nanoparticles relative to that in the pristine sample and order of carboxylic acids, derived from Mössbauer (*black columns*) and Raman (*red columns*) results.

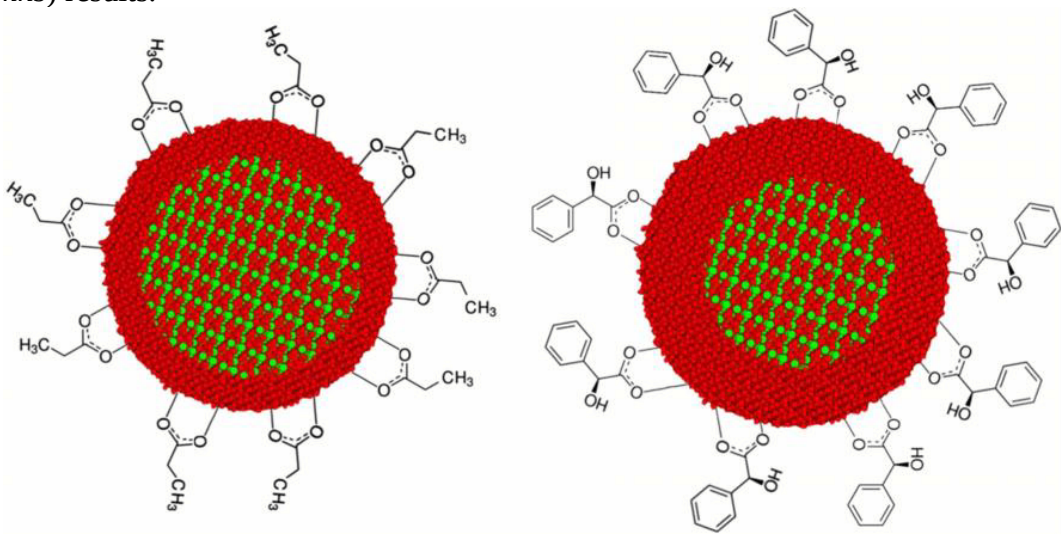

Fig. 9. Graphical schematic illustration of the effect of coating with carboxylic acids [propionic- (left) and mandelic acid (right)] on nanomagnetite as a change of the thickness of the maghemite shell.

The reason and explanation of the observed effect of carboxylic acid coating on iron oxide nanoparticles can be as follows. The oxidation of nanomagnetite can be done by oxygen (air) or by any accompanying reductive transformation of certain carboxylic acids, in our case mandelic, caprylic and lactic acids, (e.g., their conversion to aldehydes or alcohols) [54], or as an effect of noncarboxylic (i.e., hydroxylic) -OH groups. It is also possible that these acids allow (perhaps catalyze) the oxidation effected by the dissolved oxygen content of aqueous solutions. On the other hand, some carboxylic acids, in our study tartaric, propionic, glycolic, malic and caproic acids, can directly reduce the iron oxide (e.g., along with surface complexation or with electron transfer [55], perhaps oxidation of acids can occur, similarly to as it was observed with gold nanoparticles [56]). The maghemite/magnetite ratio may also depend on the formation rate of different protective layers, on the surface coverage or on other chemical parameters (like acidity), the exact mechanism of its origin is unknown yet and requests further studies.

Conclusions

Electron microscopy, photoacoustic and magnetic measurements revealed the successful two-step co-precipitation preparation of nanomagnetites coated with carboxylic acids (glycolic, propionic, lactic, malic, tartaric, citric, mandelic, caproic and caprylic) in about 10 nm size. Mössbauer spectroscopy and magnetic measurements revealed superparamagnetism of the carboxylic acid coated nanomagnetites. As of the effect of the coating, the same tendency of the changes in maghemite/magnetite ratio depending upon the nature of the different carboxylic acids was shown by ^{57}Fe Mössbauer and Raman spectroscopy in the samples. Accordingly, carboxylic acids, such as mandelic, caprylic and lactic acids, can promote oxidation of nanomagnetites, while carboxylic acids, such as tartaric, propionic, glycolic, malic and caproic acids, may promote the reduction of iron oxide nanoparticles. One of the most striking results of this research implies that Mossbauer and Raman spectroscopy results both show the same tendency in relations between the nature of carboxylic acids and maghemite/magnetite ratios. These ratios for both methods can be seen in Fig. 8 for each carboxylic acid as well as for the pristine sample. According to our results carboxylic acids, such as mandelic, caprylic and lactic acids, can promote oxidation of nanomagnetites, in contrast to carboxylic acids, such as tartaric, propionic, glycolic, malic and caproic acids, which promote the reduction of iron oxide nanoparticles. In the case of the former (oxidizing) group either the acids themselves oxidize the magnetite or allow (perhaps catalyze) the oxidation effected by the dissolved oxygen content of aqueous solutions, while in the latter (reducing) group the acids can directly reduce the surface of the iron oxide nanoparticles (e.g., along with surface complexation) [54].

Acknowledgements

This work was supported by grants of CAPES (No A127/2013) and OTKA (No K115913 and K115784). This work was carried out within the Agreement of Cooperation between Eötvös Loránd University (Budapest) and Universidade de Brasilia (Brasilia).

References

1. Radad K, Al-Shraim M, Moldzio R, Rausch WD (2012) *Environ Toxicol Pharmacol* **34**(3):661-672
2. Chen CL, Zhang H, Ye Q, Hsieh HY, Hitchens TK, Shen HH, Liu L, Wu YJ, Foley LM, Wang SJ, Ho C (2011) *Mol Imaging Biol* **5**:825-839
3. Lunacek J, Lesnak M, Jandacka P, Dvorsky R, Repkova J, Seidlerova J, Vitkovska N (2015) *Sep Sci Technol* **50**(l6):2606-2615
4. Holban AM, Grumezescu AM, Gestal MC, Mogoanta L, Mogosanu GD (2013) *Curr Org Chem* **18**(2):l85-191
5. Chandra S, Mehta S, Nigam S, Bahadur D (2010) *New J Chem* **34**:648-655
6. Sui YC, Skomski R, Sorge KD, Sellmyer DJ (2004) *J Appl Phys* **95** :715l
7. Lakshmanan R, Okoli C, Boutonnet M, Jarfis S, Rajarao GK (2013) *Bioresour Technol* **l29**:6l2-615
8. Estelrich J, Escribano E, Queralt J, Busquets MA (2015) *Int J Mol Sci* **16**:8070-8101
9. Voit W, Kim DK, Zapka W, Muhammed M, Rao KV (2001) *MRS Proceedings* (2001), vol **676**. Cambridge University Press, Cambridge
10. Albrecht T, Buhrer C, Féihnle M, Maier K, Platzek D, Reske J (1997) *Appl Phys A* **65**(2):21
11. Yildirimer L, Thanh NTK, Loizidou M, Seifalian AM (2011) *Nano Today* **6**(6):585-607
12. Soenen SJ, De Cuyper M, De Smedt SC, Braeckmans K (2012) *Methods Enzymol* 5091195-224
13. Lei L, Ling-Ling J, Yun Z, Gang L (2013) *Chin Phys B* **22**(12):127503
14. Wu W, Wu Z, Yu T, Jiang C, Kim WS (2015) *Sci Technol Adv Mater* **l6**(02350l):43
15. Khalil IM (2015) *Arab J Chem* **8**(2):279-284
16. Ray S, Nath SK, Kumar A, Agarwala RC, Agarwala V, Chaudhari GP, Daniel BSS (2009) *Adv Mater Res* **67**:221-226
17. Chen D, Ni S, Chen Z (2007) *China Particuol* **5**(5):357-358
18. Sasaki T, Zeng X, Koshizaki N (1998) *MRS Proceedings* (1998), vol **526**, Cambridge University Press, Cambridge
19. Beketov IV, Safronov AP, Medvedev AI, Alonso J, Kurlyandskaya GV, Bhagat SM (2012) *AIP Adv* **2**:022154
20. Obayemi JD, Dozie-Nwachukwu S, Danyuo Y, Odusanya OS, Anuku N, Malatesta K, Soboyejo WO (2015) *Mater Sci Eng*, C **46**(1):482-496
21. Elblbesy MAA, Madbouly AK, Hamdan TAA (2014) *Am J Nano Res Appl* **2**(5):98-103
22. Khalafalla E, Reimers G (1980) IEEE Trans Magn 161178
23. Regmi R, Black C, Sudakar C, Keyes PH, Naik R, Lawes G, Vaishnava P, Rablau C, Kahn D, Lavoie M, Garg VK, Oliveira AC (2009) *J Appl Phys* 1061113902
24. Racuciu M, Creanga DE, Airinei A, Badescu V, Apetroaie N (2007) *Magnetohydrodynamics* **43**(4):ll-18
25. de Sousa ME, Fernandez van Raap MB, Rivas PC, Zélis PM, Girardin P, Pasquevich GA, Alessandrini JL, Muraca D, Sanchez FH (2013) *J Phys Chem C* 11715436-5445
26. Soler MAG, Alcantara GB, Soares FQ, Viali WR, Sartoratto PPC, Fernandez JRL, da Silva SW, Garg VK, Oliveira AC, Morais PC (2007) *Surf Sci* **60l**(l8):392l-3925
27. Goloverda G, Jackson B, Kidd C, Kolesnichenko V (2009) *J Magn Magn Mater* **321**(10):1372-1376
28. Wei X, Wei Z, Zhang L, Liu Y, He D (2011) *J Colloid interface Sci* **354**:76-81
29. Burdukova E, lshida N, Shaddick T, Franks GV (2011) *J Colloid Interface Sci* 354182-88
30. Szekeres M, Tóth IY, Illés E, Hajdu A, Zupkó I, Farkas K, Oszlánczi G, Tiszlavicz L, Tombácz E (2013) *Int J Mol Sci* **14**:l4550-14574
31. Kazmierczaka M, Pogorzelec-Glasera K, Hilczera A, Jurgab S, Majchrzyckic L, Nowickic M, Czajkac R, Matelskic F, Pankiewiczd R, Leskad B, Kepinskie L, Andrzejewskia B (2014) *Mater Technol* **48**:59-62
32. Daou TJ, Pourroy G, Begin-Colin S, Greneche JM, Ulhaq-Bouillet C, Legare P, Bernhardt P, Leuvrey C, Rogez G (2006) *Chem Mater* 1824399-4404
33. Tang J, Myers M, Bosnick KA, Brus LE (2003) *J Phys Chem B* **l07**:750l-7506
34. Chamritski I, Burns G (2005) *J Phys Chem B* **109**:4965-4968
35. Zakharova IN, Shipilin MA, Alekseev VP, Shipilin AM (2012) *Tech Phys Lett* **38**(1):55-58 (ISSN 1063_7850)
36. Iyengar SJ, Joy M, Ghosh CK, Dey S, Kotnalad RK, Ghosha S (2014) *RSC Adv* **4**:64919-64929
37. Ozdemiar O, Dunlop DJ, Moskowitz BM (1993) *Geophys Res Lett* **20**(16):167l-1674
38. El Mendili Y, Grasset F, Randrianantoandro N, Nerambourg N, Greneche JM, Bardeau JF (2015) *J Phys Chem C* **1l9**:10662-10668

39. Santos JG, Silveira LB, Fegueredo PHS, Araufo BF, Peternele WS, Rodriguez AFR, Vilela EC, Garg VK, Oliveira AC, Azevedo RB, Morais PC (2012) *J Nanosci Nanotechnol* **12**:1-5
40. Pati SS, Singh LH, Guimaraes EM, Mantilla J, Coaquira JAH, Oliveira AC, Sharma VK, Garg VK (2016) *J Alloys Compd* **684**(5):68-74
41. Klencsar Z, Kuzmann E, Vértes A (1996) *J Radioanal Nucl Chem* **210**:105
42. Oliveira AC, Tronconi AL, Buske N, Morais PC (2002) *J Magn Magn Mater* **252**:56
43. Laurent S, Mahmoudi M (2011) *Int J Mol Epidemiol Genet* **2**(4):367-390
44. Wasilewski P, Gunther K (1999) *Geophys Res Lett* **26**(15):2275-2278
45. Kuzmann E, Nagy S, Vértes A, Weiszburg TG, Garg VK (1998) In: Vértes A, Nagy S, Süvegh K (eds) Geological and mineralogical applications of Mossbauer spectroscopy in Nuclear Methods in Mineralogy and Geology: Techniques and Applications. Plenum Press, New York, pp 285-376
46. Rumenapp C, Wagner FE, Gleich B (2015) *J Magn Magn Mater* **380**:24l-245
47. Hesse J, Rübartsch A (1974) *J Phys E* **7**:526
48. da Silva SW, Nakagomi F, Silva MS, Franco A Jr, Garg VK, Oliveira AC, Morais PC (2012) *J Nanopart Res* 141798
49. Shebanova ON, Lazor P (2003) *J Solid State Chem* 174:424-430
50. Wohlfarth EP (1980) Ferromagnetic materials: a handbook on the properties of magnetically ordered substances. Elsevier, Amsterdam
51. He YP, Miao YM, Li CR, Wang SQ, Cao L, Xie SS, Yang GZ, Zou BS, Bruda C (2005) Phys Rev B 7l:125411
52. Vargas H, Miranda LCM (1988) *Phys Rep* **161**:43
53. Frison R, Cernuto G, Cervellino A, Zaharko O, Colonna GM, Guagliardi A, Masciocchi N (2013) *Chem Mater* **25**:4820-4827
54. Mérela DS, Doa MLT, Gaillarda S, Dupaud P, Renauda JL (2015) *Coord Chem Rev* 288150-68
55. Cornell RM, Schwertmann U (2006) The iron oxides: structure, properties, reactions, Occurrences and Uses. Wiley, Cambridge
56. McEntee M, Tang W, Neurock M, Yates JT Jr (2015) *ACS Catal* **5**:744-753